Single drop impact onto a deep pool: experimental observations and theoretical model for the crater evolution

A. Bisighini*, G.E. Cossali, C. Tropea and I.V. Roisman
Facoltà di Ingegneria, Università di Bergamo, via Marconi 6, 24044 Dalmine (BG), Italy.
Technische Universität Darmstadt, Institute of Fluid Mechanics and Aerodynamics
Center of Smart Interfaces, Petersenstraße 30, 64287 Darmstadt, Germany

Abstract

An experimental investigation of the crater formed by the impact of a millimetric drop onto a semi-infinite liquid target has been performed using high-speed imaging and image processing. Then, a theoretical model for the crater evolution has been developed, which is able to predict the temporal variation of the crater depth for high Weber, Froude and Reynolds numbers. The flow around the crater is approximated by an irrotational velocity field past a moving and expanding sphere. The equations of propagation of the surface of the crater have been obtained from the balance of stresses at the crater interface, accounting for inertia, gravity, surface tension and viscosity. The temporal evolution of the crater depth has been calculated by numerical solution of the equations of motion. The model has been validated against experimental data. The agreement is rather good.

Introduction

Phenomena of drop impacts on liquid layers are related to various engineering applications in which secondary spray atomization after collision with a wall, spray deposition/coating or spray cooling play an important role. The wall flow generated by spray impact is rather complicated and is still not completely understood [1, 2, 3]. In order to model and predict the outcome of spray/wall interaction an accurate prediction of the typical sizes of the crater formed by a single drop impact and the characteristic time of its formation and collapse is necessary. Moreover, a simplified description of the liquid flow generated by drop impact is required in order to reliably model the heat transfer associated with spray cooling [4].

When a single drop impacts onto a deep pool with high velocity it creates an expanding, nearly spherical cavity. The cavity first penetrates into the liquid pool and then recedes under the action of surface tension and gravity. Most of the existing models of drop impact presented in the literature deal with predictions of the maximum crater depth. All the models, which are usually based on an energy balance, are formulated with the assumption of a hemispherical shape for the crater, centered on the impact point [5, 6, 7, 8, 9, 10, 11, 12]. [13] found an analytic expression for the crater evolution in time, using the energy balance equation and assuming a kinematically admissible irrotational flow around the expanding crater. [14] used the simple flow generated by the point source for the description of the pressure field around the crater. The equations of the crater expansion are obtained from the kinematic and dynamic boundary conditions at the free surface of the spherical crater. An analytical expression for the crater radius and depth is then obtained, which agrees well with the experimental data for the relatively early stages of crater penetration. This model does not predict maximum crater penetration depth and receding, since the surface tension and the gravity are not taken into account.

There are two main disadvantages related to most of the existing theoretical models for cavity expansion. The first problem involves the use of an *energy balance*. It is well-known that such an approach is among the lowest level theoretical tools, and can only provide appropriate and approximate scales of the problem. In the case of drop collision with a deep pool, the energy balance approach cannot easily model the energy lost due to generation of the spreading waves or the energy expended on splash and secondary atomization. The second disadvantage is in the approximation of the crater shape by an *expanding sphere with a center fixed at the impact point*. Our experiments show that such an approximation is not precise. The flow generated by an expanding sphere is symmetric, it leads to a uniform distribution of the stresses on the surface of the crater, thus it is not able to correctly describe the pressure gradient associated with gravity.

Experimental investigation

Experimental method

The impact of drops onto a pool of the same liquid has been observed using a high-speed video system. Distilled water and acetic acid were used as a working liquids. A sketch of the experimental setup is shown in

*Corresponding author: alfio.bisighini@unibg.it

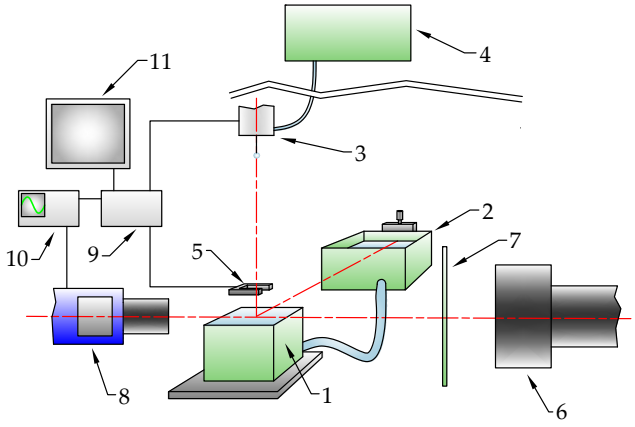

Figure 1: Schematic of the experimental setup.

Table 1: Values of density ρ, viscosity μ and surface tension σ for the fluids at the reference temperature 30 °C.

	ρ (kg/m^3)	μ (kg/ms)	σ (N/m)
Water	996	0.80×10^{-3}	71.22×10^{-3}
Acetic acid	1040	1.04×10^{-3}	26.63×10^{-3}

Figure 1. When liquid interfacial phenomena are observed through a container, the liquid meniscus formed at the interface between the liquid surface and the transparent wall obscures the area close to the interface. To avoid this effect the target pool (**1**) was placed on a level platform and was filled to the rim, using it as pinned contact line [15, 10, 11]. In order to accurately regulate the level of the water, the container was connected by a flexible tube to a liquid reservoir (**2**) mounted on a micrometric vertical stage. Drops generated with a dripper (**3**), fed by a reservoir (**4**), are detected by a light sensor (**5**). The light emitted by a lamp (**6**) is diffused by a etched glass (**7**). The components are controlled and synchronized with electronic acquisition cards (**9**), a wave generator (**10**) and a graphical user interface (**11**). The impact velocity was varied by changing the fall height. All the experiments were performed under atmospheric conditions. The camera (**8**) was mounted on a tilting, rotating and movable platform which allows adjustment of the liquid surface normal to the field of view. The target fluid is heated up due to the high intensity illumination, its temperature remains constant at 30 °C. The physical properties of the liquids at this temperature are reported in Table 1. Image analysis was run together with a graphical interface showing frame by frame the edges of the detected features superimposed onto the original image and allowing visual user control. Correct configuration and image analysis, which accounts for the effects related to the refraction, are rather important in order to obtain reliable data. More details can be found in [16].

Five selected cases are presented in Table 2. The Weber, Froude and Reynolds numbers are used in this study to describe the phenomena of drop impact: We $= \rho V^2 D/\sigma$, Fr $= V^2/(gD)$ and Re $= \rho V D/\mu$, where ρ, μ, σ are the density, the viscosity and the surface tension of the target liquid, D and V are the diameter and velocity of the impacting drop. Some variables and parameters in this study will be presented in dimensionless form. They are scaled using D as the length scale, V as the velocity scale, and D/V as the time scale. Δ and Ω are used to represent the dimensionless crater depth and width, while τ is the dimensionless time.

Experimental results

A typical time sequence of drop impact is shown in Fig. 3. The crater and the crown reach their maximum size at about the same time. Then the crown begins to fall down, generating capillary waves which travel to the bottom of the receding crater, from which a central jet is ejected.

Figure 3a show the evolution in time of the dimensionless crater depth Δ. At smaller Weber numbers, corresponding to the cases *a* and *b*, the effect of surface tension is significant and the evolution of the crater is soon

Table 2: List of impact parameters and the results for the dimensionless maximum crater depth $\Delta_{\max}$ and the corresponding instant $\tau_{\max}$. Case *d* is shown in Figure 3.

Case	Fluid	D (mm)	V (m/s)	We	Fr	Re	$\Delta_{\max}$	$\tau_{\max}$
a	water	2.2	2.4	170	262	6391	2.44	14.83
b	water	1.8	3.0	226	489	6774	2.55	17.48
c	water	2.3	3.6	406	569	10 128	2.82	20.54
d	water	2.8	4.2	683	620	14 638	2.93	22.01
e	acetic acid	2.9	4.4	2190	694	12 687	3.11	27.08

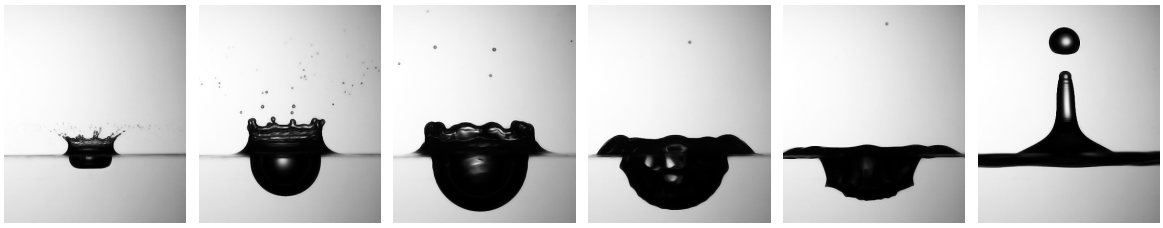

(a) $t = 1.3$ ms (b) $t = 4.3$ ms (c) $t = 10.4$ ms (d) $t = 22.6$ ms (e) $t = 28.7$ ms (f) $t = 78.8$ ms

Figure 2: Drop impact in the splashing regime. (Water, $D = 2.8\,\mathrm{mm}$, $V = 4.2\,\mathrm{m/s}$, We $= 688$, Fr $= 619$, Re $= 14\,624$).

influenced by the propagation of the capillary waves. The curves corresponding to higher Weber numbers, see cases *c* - *e*, are rather smooth, which indicates that the evolution of the crater is influenced by the capillary waves only at longer times. Due to a different behavior of depth and width evolution, the shape factor $\epsilon = \Delta/\Omega$ of the crater is not constant, but varies in time, as shown in Figure 3b. It is also obvious that the crater is not a perfect hemisphere, with its center at the impact point (which would correspond to $\epsilon = 1/2$), as considered in all of the previous analytical models.

Model development

In order to develop a simplified model for crater formation, we subdivided the process of drop impact into two main phases. During the first phase, $\tau < \tau^*$ (τ being the dimensionless time), the drop deforms, generating a thin radially expanding liquid layer. The motion of this interface is governed by the balance of the stresses generated by the flows of the drop and pool liquids. The velocity of penetration of the drop/target interface at the time period $\tau < \tau^*$, is approximately half of the impact velocity. This result is well-known from the penetration mechanics [17, 18] and was previously used for the description of drop impact [12, 14]. The dimensionless rate of drop erosion is therefore approximately $1/2$. The typical dimensionless time of drop deformation is thus $\tau^* \approx 2$.

At times $\tau > \tau^*$, a thin residual liquid layer of the drop material is formed on the crater surface. During this phase the cavity shape can be well approximated by the shape of the drop/target interface. The inertial effects associated with the flow in this layer are negligibly small and the dynamics of cavity expansion can be analyzed involving conventional boundary conditions of a free surface. Crater expansion is governed by the inertia of the flow in the liquid pool and decelerated by capillary forces and gravity.

At some instant the crater reaches a maximum penetration depth and starts to recede. At relatively small Weber numbers, the receding phase is influenced significantly by the capillary waves generated by the falling crown. Moreover a jet is ejected from the center of the crater. These phenomena affect significantly the dynamics of cavity collapsing. Their analysis is outside the scope of the present study.

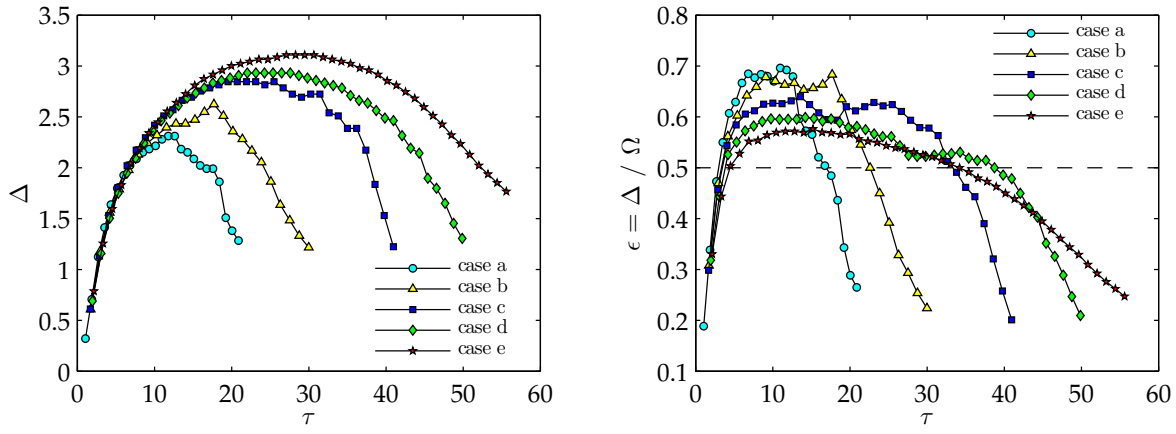

(a) (b)

Figure 3: Measurements of the dimensionless crater depth Δ and width shape factor ϵ as a function of the dimensionless time τ. Impact conditions have been reported in Table 2.

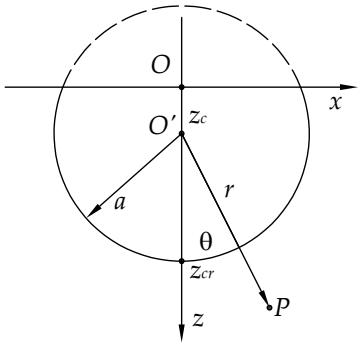

Figure 4: Sketch of the cavity and definition of the fixed and moving reference frames.

Flow field in the liquid pool

In this study the cavity expansion is approximated by a combination of the sphere expansion and its translation along the impact axis.

Consider a reference frame fixed at the impact point O with the x axis lying on the unperturbed liquid surface and the z axis (impact axis) directed normal to it, as in Figure 4. Consider also a moving spherical coordinate system $\{r, \theta, \varphi\}$ with the origin at the center O′ of the spherical cavity, where r is the radial coordinate and θ is the zenith angle. The radius of the crater in the relative spherical reference system is denoted by $a(t)$ and the position of its center on the symmetry axis by $z_c(t)$.

The potential ϕ of a relative irrotational flow around the cavity in the moving coordinate system satisfying the Laplace equation $\Delta\phi = 0$ can be easily obtained as a superposition of a flow past a sphere and the radially expanding flow generated by sphere expansion:

$$\phi = -\dot{z}_c r \left(1 - \frac{a^3}{2r^3}\right) \cos\theta - \dot{a}\frac{a^2}{r}. \tag{1}$$

The pressure distribution $p_{\rm cr}(\theta, t)$ in the liquid at the crater surface, $r = a$, can be obtained using the nonstationary Bernoulli equation [19]:

$$\frac{p_{\rm cr}}{\rho} = \frac{U^2}{2}\left(1 - \frac{9}{4}\sin^2\theta\right) + g(z_c + a\cos\theta) + \frac{a\dot{U}}{2}\cos\theta + \frac{3\dot{a}^2}{2} + a\ddot{a} + \frac{3}{2}\dot{a}U\cos\theta. \tag{2}$$

It contains two unknown functions, $a(t)$ and $z_c(t)$, which have to be determined from the dynamic boundary conditions at the crater surface accounting for the capillary forces and gravity.

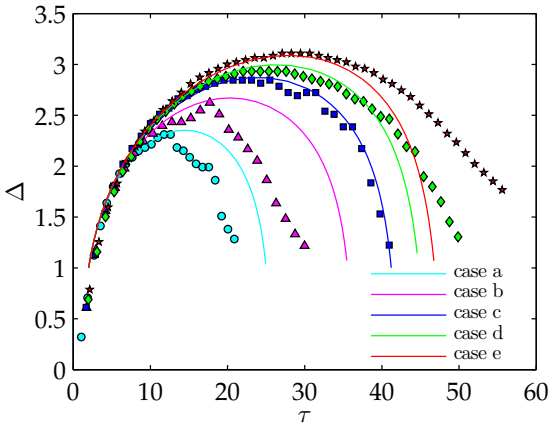

Figure 5: The dimensionless depth of crater penetration as a function of the dimensionless time. Comparison between experimental data (symbols) and theoretical predictions (curves) for various impact parameters listed in Table 2.

Crater evolution at times $t > 2D/V$

At large times the pressure gradient in the thin drop spreading on the expanding crater is negligibly small. The Young-Laplace equation applied to the crater surface, $p_{\rm cr} + 2\sigma/a = 0$, cannot be satisfied exactly over the entire cavity surface. On the other hand expression (2) can be linearized near the cavity bottom, $\theta \approx 0$. The dynamic boundary condition can then be written in the form:

$$0 = -\frac{7U^2}{4} + gz_c + \frac{3\dot{a}^2}{2} + a\ddot{a} + \frac{2\sigma}{\rho a} + \left[\frac{9U^2}{4} + ga + \frac{a\dot{U}}{2} + \frac{3\dot{a}U}{2}\right]\cos\theta + O(U^2\theta^4). \tag{3}$$

It should be noted that at large times $U \ll \dot{a}$ since in all the considered cases the Froude number is small, therefore the last term in (3) is negligibly small in comparison with other terms.

Denote the dimensionless crater radius and axial coordinate of the center of the sphere as α and ζ. The dimensionless penetration depth is expressed as $\Delta = \zeta + \alpha$. Condition (3) yields the dimensionless system of ordinary differential equations for $\alpha(\tau)$ and $\zeta(\tau)$:

$$\ddot{\alpha} = -\frac{3}{2}\frac{\dot{\alpha}^2}{\alpha} - \frac{2}{\alpha^2 \mathrm{We}} - \frac{1}{\mathrm{Fr}}\frac{\zeta}{\alpha} + \frac{7}{4}\frac{\dot{\zeta}^2}{\alpha} - \frac{4\dot{\alpha}}{\alpha^2 \mathrm{Re}}, \tag{4}$$

$$\ddot{\zeta} = -3\frac{\dot{\alpha}\dot{\zeta}}{\alpha} - \frac{9}{2}\frac{\dot{\zeta}^2}{\alpha} - \frac{2}{\mathrm{Fr}} - \frac{12\dot{\zeta}}{\alpha^2 \mathrm{Re}}. \tag{5}$$

where the effect of viscosity has also been included. Since the order of the magnitude of $\dot{\alpha}$ is comparable with unity the importance of the viscous terms in (4) in comparison with the capillary forces can be estimated by the capillary number $\mathrm{Ca} = \mathrm{Re}/\mathrm{We}$. The present analysis is therefore valid for the cases when the effect of viscous forces is small, i.e. for $\mathrm{Ca} \gg 1$. The evolution of the crater can now be evaluated by numerical integration of the system of ordinary differential equations (4)-(5) subjected to the initial conditions, obtained from experimental data and theoretical predictions (for further details see [19]).

Results and discussion

A comparisons between the model prediction and experiments for evolution of the penetration depth are shown in Figure 5. The agreement is rather good. As expected, the difference between experimental data and predicted values increases at the last part of the receding phase. Some discrepancy between the predictions and the experiments can be explained by the influence on the flow of the propagating capillary waves (not considered in the theory) and by the crater deformation at the bottom part, leading to the formation of the central jet. Cases *a* and *b* in Figure 5 correspond to low impact velocity at which capillary waves soon significantly deform the crater shape.

Figure 6 shows a superposition of the crater predicted by the theoretical model to the recorded images for the case *d* of Table 2. The agreement between the theoretical predictions and the experimental shape of the cavity is rather good at the bottom region of the crater ($\theta \ll 1$) where the model is valid. Some discrepancy appears when the shape of the crater is deformed by the capillary waves.

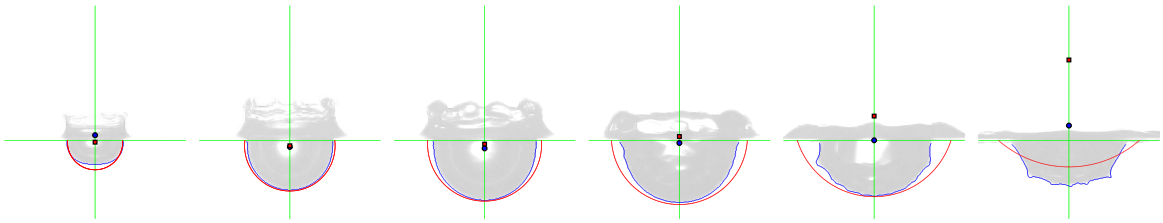

(a) $\tau = 3.02$ (b) $\tau = 9.72$ (c) $\tau = 17.54$ (d) $\tau = 27.60$ (e) $\tau = 37.65$ (f) $\tau = 44.36$

Figure 6: Superposition of the theoretical model and the recorded images. The round symbol represents the center of the circle fitting the crater profile. The square symbol represents the center of the modeled crater.

Conclusions

An experimental and analytical investigation of the crater formed by the impact of a drop onto a deep liquid pool at sufficiently high Weber, Froude and Reynolds numbers has been presented. Image processing has revealed the shape of the crater to be very similar to a portion of a sphere. Potential flow theory has been used to model the flow around the crater. The equations of cavity expansion have been obtained from the balance of stresses at the crater interface. The model accounts for the effects of inertia, gravity and surface tension. It is shown that at high Reynolds numbers, especially if Re $>$ We, the effect of viscosity is negligibly small. The agreement between the theoretical predictions and the experimental data for the evolution of the penetration depth of the cavity is rather good. The proposed approach can be potentially used for the description of impact of small sub-millimeter drops typical for spray/wall interaction, in which the effect of capillary forces is significant.

Acknowledgement

A.B. acknowledges financial support of Cariplo, DAAD and COST P21. G.E.C. acknowledges the partial funding from the National Project PRIN07. C.T. and I.V.R. would like to thank German Science Foundation (DFG) for financial support by the research grant No. Tr 194/34, the research grant in the framework of the Collaborative Research Center 568 (TP A1) and the Center of Smart Interfaces (EXCL 259).

References

[1] Panao, M.R.O. and Moreira, A.L.N., *Experiments in Fluids* 39:364-374 (2005).
[2] Roisman, I.V., Horvat, K. and Tropea, C., *Physics of Fluids* 18:102-104 (2006).
[3] Schneider, L., Le Lostec, N., Villedieu, Ph. and Sadiki, A., *International Journal of Multiphase Flow* 36:261-272 (2010).
[4] Visaria, M. and Mudawar, I., *International Journal of Heat and Mass Transfer* 51:2398-2410 (2008).
[5] Engel, O.G., *Journal of Applied Physics* 37:1798-1808 (1966).
[6] Olevson, K.L.R., *US Geological Survey Research* 650:D189-D194 (1969).
[7] Macklin, W.C. and Metaxas, G.J., *Journal of Applied Physics* 47:3963-3970 (1976).
[8] Pumphrey, H.C. and Elmore, P.A., *Journal of Fluid Mechanics* 220:539-527 (1990).
[9] Prosperetti, A. and Oguz H.N., *Annual Review of Fluid Mechanics* 25:577-602 (1993).
[10] Liow, J.L., *Journal of Fluid Mechanics* 427:73-105 (2001).
[11] Brutin, D., *Comptes Rendus Mecanique* 331:61-67 (2003).
[12] Fedorchenko, A.I. and Wang A.B., *Physics of Fluids* 16:1349-1365 (2004).
[13] Engel, O.G., *Journal of Applied Physics* 38:3935-3940 (1967).
[14] Berberovic E., van Hinsberg N.P., Jakirlic S., Roisman, I.V., and Tropea, C., *Physics Review E* 79:036306 (2009).
[15] Rein, M., *Journal of Fluid Mechanics* 306:145-165 (1996).
[16] Bisighini, A., *Ph.D. Thesis - University of Bergamo* (2010).
[17] Birkhoff, G., MacDougall, D.P., Pugh, E.M. and Taylor, G., *Journal of Applied Physics* 19:563 (1948).
[18] Yarin, A.L., Rubin, M.B. and Roisman, I.V., *International Journal of Impact Engineering* 16:801 (1995).
[19] Bisighini, A., Cossali, G.E., Tropea, C. and Roisman, I.V., *Physiscs Review E* almost accepted (2010).